Sensor properties of plasmonic silver and gold nanoparticles produced by pulsed laser deposition

ILHAN CANDAN[1], SERAP YIGIT GEZGIN[2], HADICE BUDAK GUMGUM[1], HAMDI SUKUR KILIC[2,3,4,*]
[1]*Department of Physics, Faculty of Science, Dicle University, 21280 Diyarbakir, Turkey*
[2]*Department of Physics, Faculty of Science, University of Selcuk, 42031 Selcuklu, Konya, Turkey*
[3]*Directorate of High Technology Research and Application Center, University of Selcuk, 42031 Selcuklu, Konya, Turkey*
[4]*Directorate of Laser-Induced Proton Therapy Application and Research Center, University of Selçuk, 42031 Konya, Turkey*

In this study, 20-100 nm Au and Ag noble metal nanoparticles were produced using the Pulse Laser Deposition technique, and very sensitive optical properties of nanoparticles were investigated using the LSPR technique. The morphology of the produced nanoparticles was determined and characterized using scanning electron microscopy (SEM). The chemical bond structure of the Biotin molecule was investigated by Fourier Transform Infrared Spectroscopy (FTIR). In addition, the UV-Vis spectroscopy technique was used to determine LSPR absorption peaks of nanoparticles. Au and Ag Nanoparticles were deposited on the glass substrate depending on the laser deposition times. As the laser deposition time of the produced nanoparticles increased, both the size of the formed nanoparticles and the number of nanoparticles per unit surface increased. It was observed that the shape of Au and Ag nanoparticles produced based on SEM images was spherical. When UV-Vis spectra of Au and Ag nanoparticles were examined, it was observed that LSPR peaks shifted to longer wavelengths (redshift) as the laser deposition times increased. We have observed, to our knowledge, that the highest LSPR peak appeared at 1065 nm in the near-infrared region for plasmonic Au nanoparticles produced by Pulsed Laser Deposition. Once LSPR peaks of the plasmonic nanoparticles were characterized, Biotin molecules with different concentrations were attached to Ag and Au NPs to detect the sensor properties. LSPR peak shifts of bound nanoparticles could be observed and a blueshift of peaks was demonstrated as the concentration increased.

(Received November 26, 2023; accepted June 3, 2024)

Keywords: Au, Ag, Plasmonic Nanoparticles, Sensor, LSPR, PLD

1. Introduction

Plasmonic nanoparticles (P-NPs) have been studied extensively by several science groups in the last two decades. When noble metal nanoparticles (NPs) interact with light, free electrons on the metal surface are forced to oscillate and surface plasmon resonance (SPR) occurs at a certain wavelength. This enormous optical phenomenon is a very delicate process and depends on the size, shape, and surrounding environment of NPs. Notable for their small size, high surface area/volume ratio, and strong absorption coefficients, NPs are of great interest in analytical chemistry [1, 2]. Metal analytical techniques based on NPs have become increasingly important and widely used for detection due to their high sensitivity, wide linear range, and simple structure in the clinical, pharmaceutical, environmental, and food safety fields. Therefore, metal nanostructures are of great interest, both fundamentally and technologically, due to their many unique properties and functionalities compared to their bulk counterparts. One of the most important aspects of NPs is their optical properties. Many metal structures such as nanoscaled silver and gold exhibit strong absorption in the optical Vis region in the spectrum compared to their bulk structures. The absorption peaks of Au and Ag elements are around 530 and 400 nm, respectively. These optical properties of nanoscale metal particles depend on various parameters such as their size [3], shape [4], the composition of the metal [5], and the surrounding environment of the particles [6-10]. Plasmonic metal nanostructures' optical properties are fundamental; therefore, they have attracted very strong attention from many research groups in recent years [11]. Changes in wavelength (colour) position of the absorption peak of NPs are due to changes in shape, size distribution, and environment, and these substances cause their transition from the Vis to NIR regions in the spectrum as inorganic chromophores. In this way, researchers have studied various applications of metal nanostructures as optical sensors and imaging tools [12-14]. For example, nowadays the application of nanomaterials as optical sensors is similarly considered an excellent candidate for detecting biological impurities such as the presence of Escherichia coli in water [15, 16]. The reason for using P-NPs as sensors is their ability to amplify signals very well. Noble metals, especially gold (Au) and silver (Ag) NPs show unique and tunable plasmonic resonance properties. The size, shape, and response of these metal nanostructures to the local environment can be controlled, and changes in wavelength can be measured by shifts in Localised Surface Plasmon Resonance (LSPR) peaks.

Metal nanoparticles (MNPs) play an important role in many different fields. They can serve as a model system to experimentally investigate quantum confinement and its effects on magnetic, electronic, and other related

properties [17, 18]. MNPs are also used in many fields such as catalysis [19], photography [20], biological labeling [21], photonics [22], optoelectronics [23], information storage [24], and Surface Enhanced Raman Scattering (SERS) [25, 26]. MNPs can be produced by various methods such as electrochemical methods, decomposition of organometallic precursors, and reduction of metal salts in the presence of stabilizers or vapor deposition methods, especially Laser Ablation (LA) and Pulsed Laser Deposition (PLD) techniques [27]. Among these techniques, the size and density of NPs can be adjusted at the desired scale by easily controlling the parameters of the PLD system such as laser fluency, laser wavelength, laser pulse number, laser pulse duration, background gas pressure, and distance between target and substrate. Thanks to these distinguishable features of PLD, the movement of LSPR peaks of P-NPs in the short or long wavelength direction of the solar spectrum can be easily achieved[28, 29]. The PLD technique was employed in this work to control the optical properties of P-NPs[30].

Biotin, categorized as a B-complex vitamin, is a water-soluble essential nutrient. Its recognition as a vitamin took almost four decades of research [31-33]. While all living organisms require biotin, only certain bacteria, yeasts, molds, algae, and some plant species can synthesize it [31]. Also known as vitamin H, biotin acts as a crucial coenzyme, displaying biological activity when linked covalently to biotin carboxylases, a group of vital enzymes involved in fatty acid biosynthesis, gluconeogenesis, and propionate catabolism [34, 35]. In 1936, it was initially identified as a growth factor for yeast in its methyl ester form. Structurally, the molecule features a bicyclic ring system with a valeric acid side chain that breaks its mirror symmetry. This system contains a ureido ring on top and a sulphur-containing tetrahydrothiophene (or thiophane) ring at the bottom. Biotin also includes three consecutive stereocenters on the thiophane ring in the all-cis configuration [36]. In this study, we employed Biotin molecules as analytes that were bonded to the surface of plasmonic Au and Ag NPs.

In our paper, we examined plasmonic Au and Ag NPs produced by the PLD technique. The LSPR peaks of produced P-NPs were determined by UV-Vis spectroscopy. The morphological properties of NPs were investigated by Scanning Electron Microscopy (SEM) and Energy Dispersive Spectroscopy (EDS). Fourier Transform Infrared Spectroscopy (FTIR) was employed to reveal the vibrational properties of the Biotin molecule. Different concentrations of Biotin molecules were bonded to the surface of the plasmonic Au and Ag NPs to investigate the sensor properties via LSPR peak shift. Additionally, the produced plasmonic Au NPs exhibited an LSPR peak at the near-infrared (NIR) region up to 1065 nm which is the highest to our knowledge. In particular, this high LSPR peak of Au NP thin films produced by the PLD technique has not been reported so far in the literature. Such a peak at the NIR range of spectrum could potentially be employed in the production of photovoltaic (PV) devices to enhance the efficiency in that region.

2. Experimental setup

The PLD system was employed to synthesize silver and gold NPs. A pulsed mode Nd: YAG laser system with a wavelength of 1064 nm, lasting 5 ns and repeating at 10 Hz, was utilized for the process. The laser system can produce second, third, and fourth harmonics at 532, 355, and 266 nm, respectively, when the fundamental wavelength is 1064 nm. For this study, the fundamental wavelength of 1064 nm was employed. Before focusing the laser with a lens, a neutral density filter was used to regulate the laser pulse power, as illustrated in Fig. 1a. The substrate used for depositing Ag and Au NPs was a glass microscope slide, which was thoroughly cleaned by applying soap suds and subsequently washing it with isopropyl alcohol and acetone, with each step taking 15 minutes. The cleaning process was further enhanced by placing the substrates in an ultrasonic bath. Lastly, a stream of nitrogen gas was employed to dry substrates.

In our experiment, we used commercially available high-purity Ag and Au sputtering targets (99.99%, Plasmaterials, USA). To avoid any damaging effects on the targets, the targets and substrate were placed on two independently rotating holders. Since each laser pulse hits a different place on the target, a homogeneous coating was obtained after LS as shown in Fig. 1. A fixed distance of 5 cm was applied between the target and substrate parts. Then, laser deposition was performed for all films at room temperature. The energy of the laser was set at 35 mJ per pulse (Au NPs were set at 20 mJ) and the laser beam was focused on Ag and Au targets using a 50 cm focal length lens. The angle of the laser beam was fixed at 450 on the target surface. Experiments were conducted in an ultra-high vacuum of about 5×10^{-7} mbar. The gold and silver sputtering targets were ablated by applying different numbers of laser pulses for different NP production. The produced Au and Ag NP plasma were illustrated in Fig. 2a. Au(1), Au(2), Au(3), Au(4), and Au(5) NPs are corresponding to 3000, 6000, 1200, 3600, and 20400 laser pulse numbers, respectively. Ag(1), Ag(2), Ag(3), Ag(4), and Ag(5) NPs are corresponding to 1800, 3600, 5400, 7200, and 9000 laser pulse numbers, respectively. The morphologies of produced Ag and Au NPs were analyzed by SEM measurement, and then EDX spectra were taken to investigate the elemental composition of the thin film. Absorption spectra of Ag and Au NPs were determined using a UV-Vis spectrometer (V-670 Jasco, USA). Additionally, FTIR spectroscopy was used to determine the Biotin spectrum. 10-60 ppm biotin (Sigma-Aldrich) solution was used to investigate the sensor properties of the produced P-NPs (Fig. 2b). Ultrapure water was used as a solvent. A 60 ppm solution of biotin (Sigma-Aldrich) molecule was prepared in pure water. Afterward, this solution was diluted with ultrapure water until 50, 40, 30, 20, and 10 ppm concentrations were obtained, respectively, and prepared to be added to the surfaces of Au and Ag NPs. LSPR peak shifts of plasmonic Ag and Au NPs were measured by UV-Vis spectrometry.

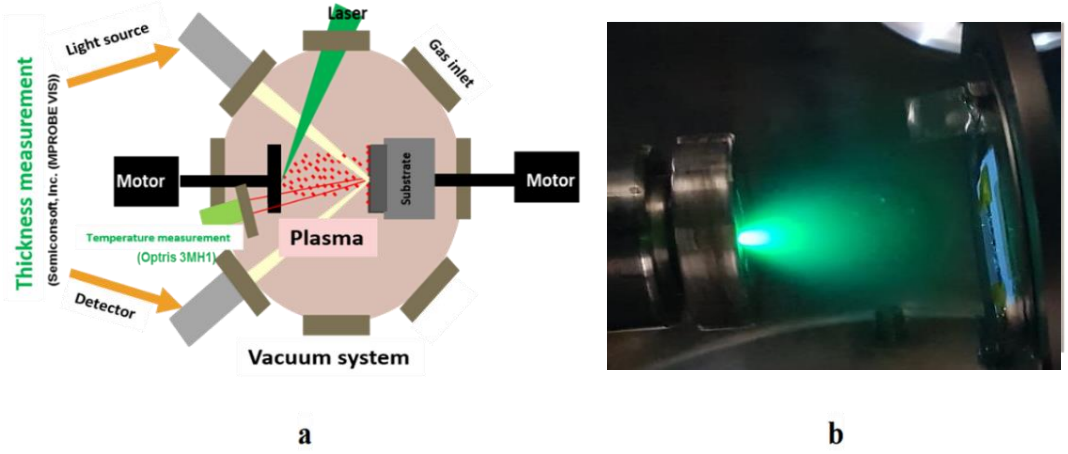

Fig. 1. (a) The diagram illustrates the locally designed and produced PLD system by the the Selcuk University Laser Spectroscopy Group; (b) The PLD system is utilized to ablate the plasma of the Ag target material [37] (color online)

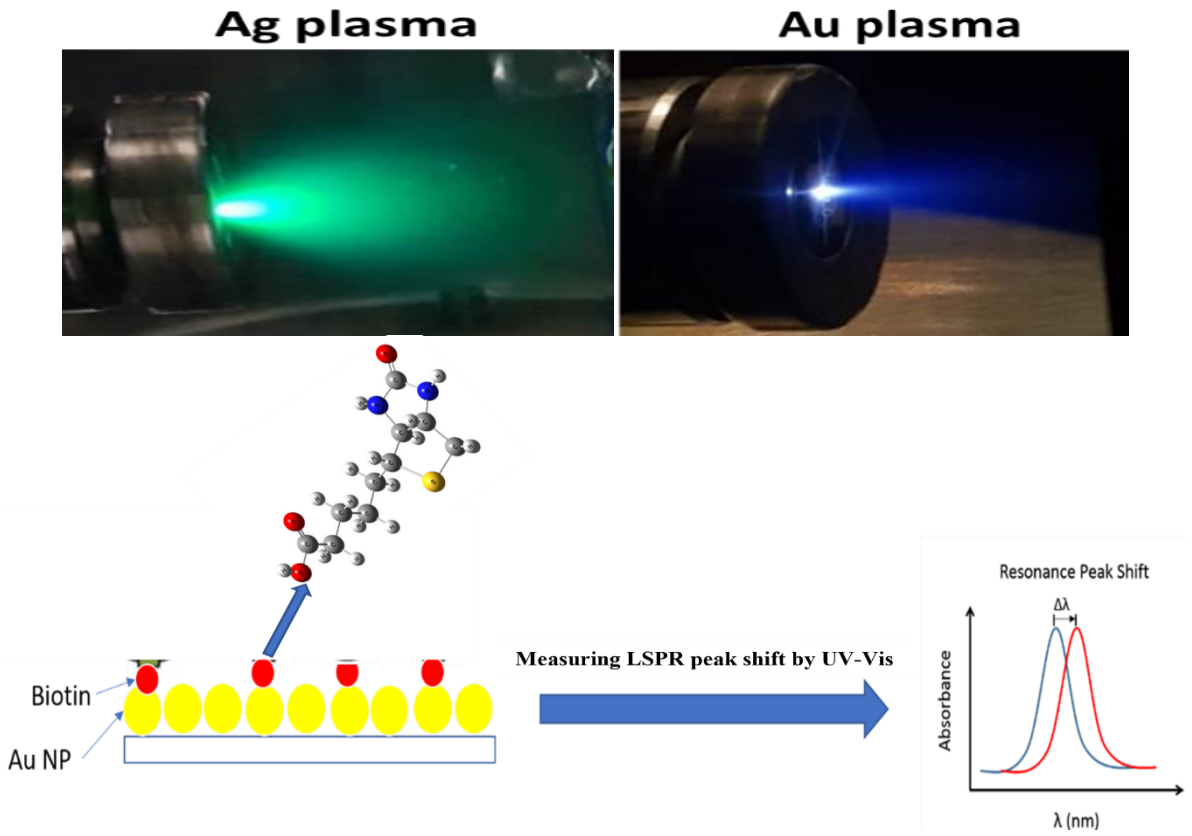

Fig. 2. (a) Laboratory view of Ag (green colour) and Au (blueish colour) nanoparticles' plasma, (b) Representation of Au-Biotin bonding and LSPR peak shift (color online)

3. Results and discussion

The absorption spectra and SEM images of Ag and Au NP thin films grown depending on the number of laser pulses in small squares are given in Fig. 3a and 3b, respectively. While the number of laser pulses was increased, LSPR peaks of NP thin films shifted towards to longer wavelength region. This redshift is based on enlarge in sizes of Ag and Au NPs [38-41]. LSPR peak of Ag NPs (Ag1) has an average particle size of 100 nm that is on 482 nm wavelength, as seen in Fig 3a. When the average size of Ag NPs (Ag5) rose to ~200 nm, their LSPR peak shifted to 742 nm wavelength. To ~120 nm particle size of Au NPs (Au2), their LSPR peak is at 684 nm wavelength in Fig 2b. With some increase in laser energy, the particle size (Au5) rose to ~225 nm and the LSPR peak shifted to 1065 nm wavelength.

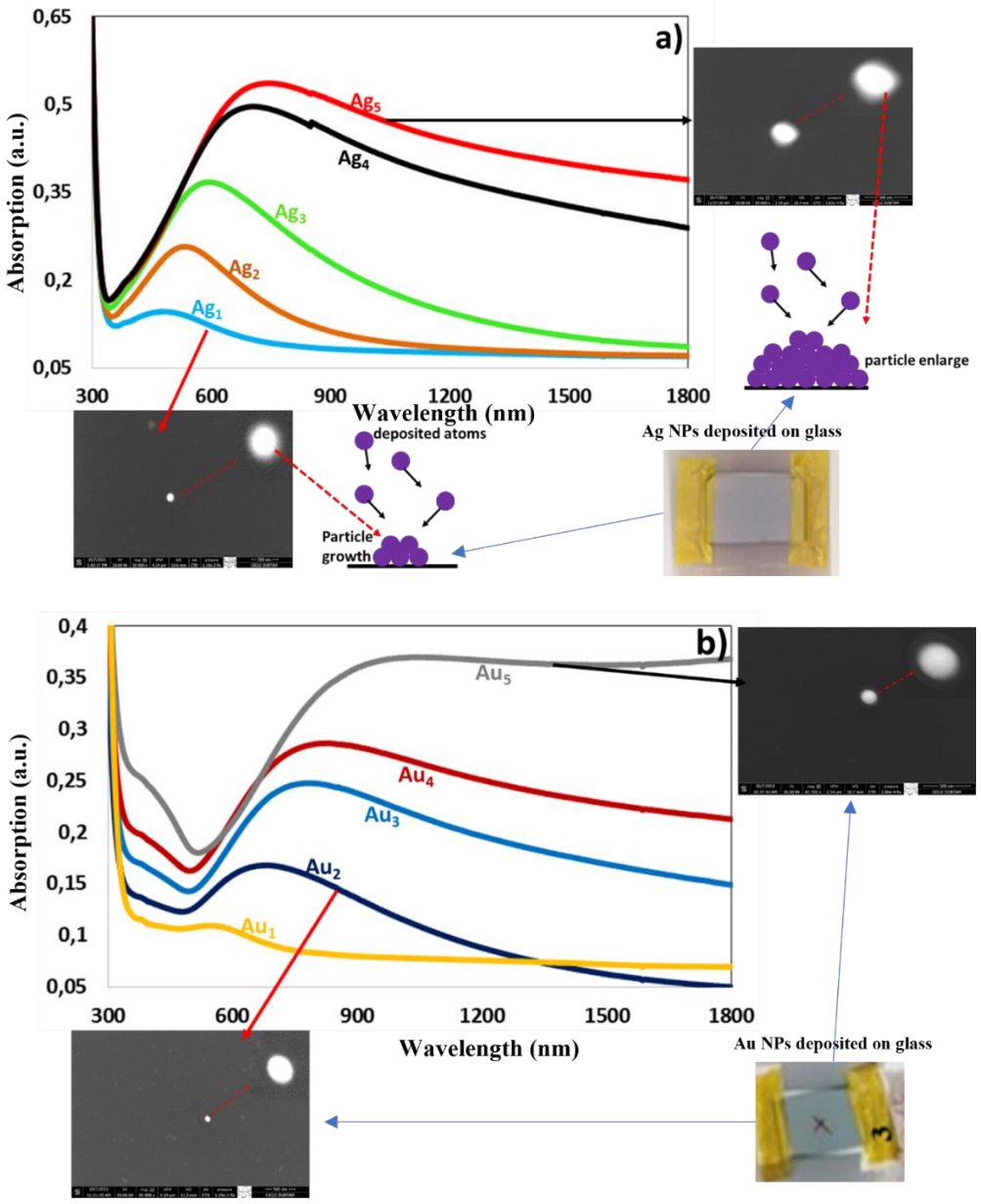

Fig. 3. Effect of laser pulse number on LSPR positions of Ag and Au NPs (color online)

The graphs of LSPR wavelengths of all Ag and Au NPs depending on the number of laser pulses are given in Fig. 3. The red shift in the LSPR peak due to the width of particle size can be explained as follows: As the number of laser pulses increased, the amount of deposition enhanced as the number of particles deposited on the substrate increased[42]. Since the number of atoms stacked side by side and on top of each other increased, the nucleation increased and the particle size widened [43, 44]. As the size of Ag NPs widens, the electric field across the particle cannot be uniform due to the size of the NP approaching the wavelength of the incident light. Thus, the field of light is disturbed across the particle and the polarization on the particle surface tends to break down. The distance between opposite charges at the particle's sides increases and thus the restoring forces between opposite charges decrease[45]. Therefore, the movement of the synchronously oscillating plasmons is disturbed and phase retardation is occurred. Due to the phase retardation, the resonance frequency and energy decreased, thus LSPR wavelength increased [46, 47].

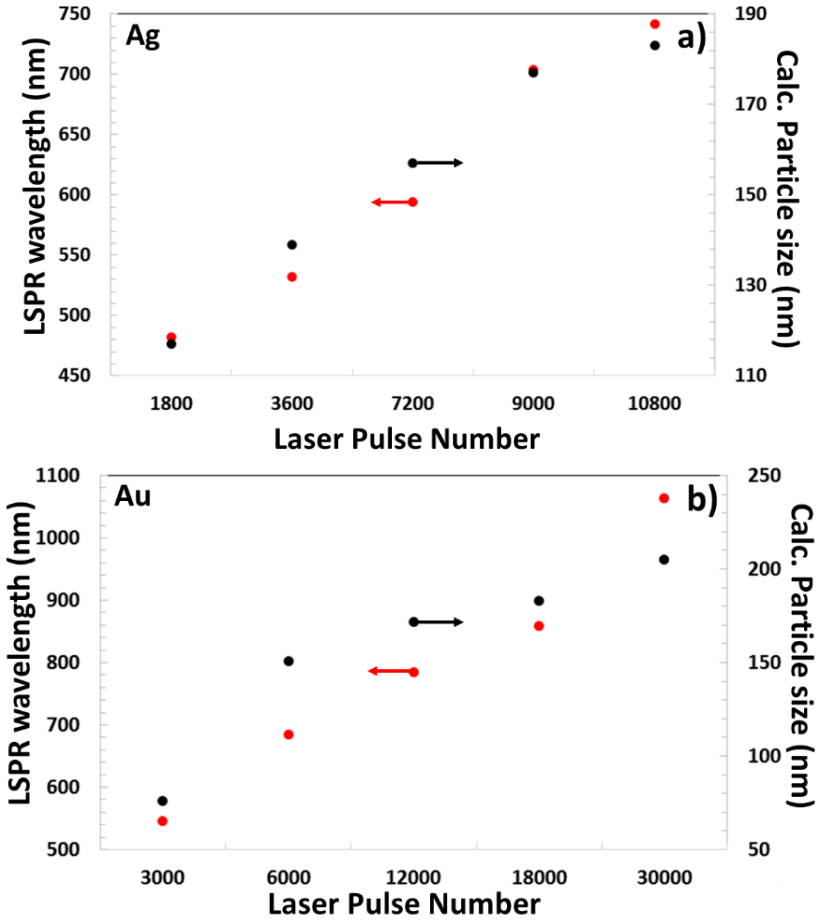

Fig. 4. LSPR wavelength and calculated particle size variation of a) Ag and b) Au NPs based on laser pulse number (color online)

The size of plasmonic NP is calculated based on LSPR wavelength, using Equation (Eq. 1):

$$d = \frac{ln\left(\frac{\lambda_{LSPR}-\lambda_o}{L_1}\right)}{L_2} \quad (1)$$

where, $\lambda_o = 400$ nm for Ag NP; 512 nm for Au NP, $L_1 = 6.53$ and $L_2 = 0.0216$ [48]. Using Eq. (1), theoretically calculated sizes of Ag NPs are given in the Table 1. The average size of Ag1 and Ag5; Au2 and Au5 NPs determined from SEM images (in 500 nm bar) in small square inserts in Fig. 3a and Fig. 3b, respectively. Experimentally measured and theoretically calculated NP sizes are close to each other.

Table 1. LSPR wavelengths and calculated particle sizes of Ag and Au NPs

Sample NP thin films	LSPR wavelength	Calculated particle size	Sample NP thin films	LSPR wavelength	Calculated particle size
Ag1	482 nm	117 nm	**Au1**	546 nm	76 nm
Ag2	532 nm	139 nm	**Au2**	684 nm	151 nm
Ag3	594 nm	157 nm	**Au3**	784 nm	172 nm
Ag4	704 nm	177 nm	**Au4**	858 nm	183 nm
Ag6	742 nm	183 nm	**Au6**	1064 nm	205 nm

3.1. Binding of Biotin to Ag NPs

Ag NPs were produced after 12 minutes (7200 laser pulses) of laser deposition. Different concentrations of Biotin molecules were attached to determine the sensor properties of Ag NPs produced by the PLD mechanism. The first, 10, 20, 30, 40, 50, and 60 ppm Biotin solutions were prepared in distilled water. Before binding the biotin molecule to Ag NPs, pure water was added to the produced film surface, and the absorption spectrum was taken by UV-Vis-NIR spectroscopy. Then, by adding different concentrations of Biotin molecules to Ag NPs, the spectra were taken and the shift amounts were determined.

In Fig. 5, only LSPR peaks obtained by adding Ag NP, and distilled water with different concentrations of Ag NP and Biotin molecule are seen. In Fig. 5, it is seen that the peaks formed in the LSPR spectrum obtained by adding distilled water and 10, 20, 30, 40, 50, and 60 ppm Biotin molecules with Ag NP for 12 minutes (7200 laser pulses) shift to the low wavelength region.

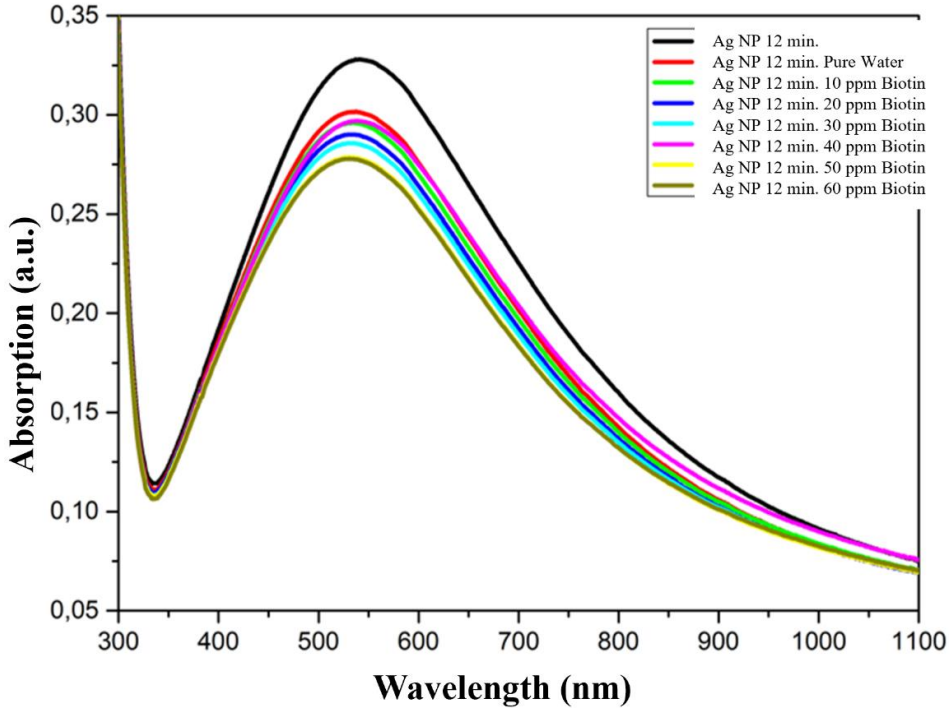

Fig. 5. Biotin interaction with silver nanoparticles (Ag NPs) leads to a blue-shift in the Localized Surface Plasmon Resonance (LSPR) peaks (color online)

Table 2. LSPR peak shifts of Ag NPs due to Biotin concentration change

Element and Deposition time	**Bound molecule**	**Concentration (ppm)**	**Number of laser pulses**	**NP Shape**	**LSPR Peak (nm)**	**$\Delta\lambda$(nm)**
Ag NP 12 min.	-	-	7200	Spherical	540	Reference peak
Ag NP 12 min.	Pure water	-	7200	Spherical	529	11
Ag NP 12 min.	Biotin	10	7200	Spherical	525	15
Ag NP 12 min.	Biotin	20	7200	Spherical	520	20
Ag NP 12 min.	Biotin	30	7200	Spherical	517	23
Ag NP 12 min.	Biotin	40	7200	Spherical	505	15
Ag NP 12 min.	Biotin	50	7200	Spherical	517	23
Ag NP 12 min.	Biotin	60	7200	Spherical	517	23

Fig. 6b shows the LSPR spectrum obtained by adding distilled water and 10, 20, and 30 ppm biotin molecules with Ag NP for 12 minutes (7200 laser pulses). LSPR peaks formed after the addition of pure water and biotin to Ag NPs shifted to blue and moved to the lower wavelength region.

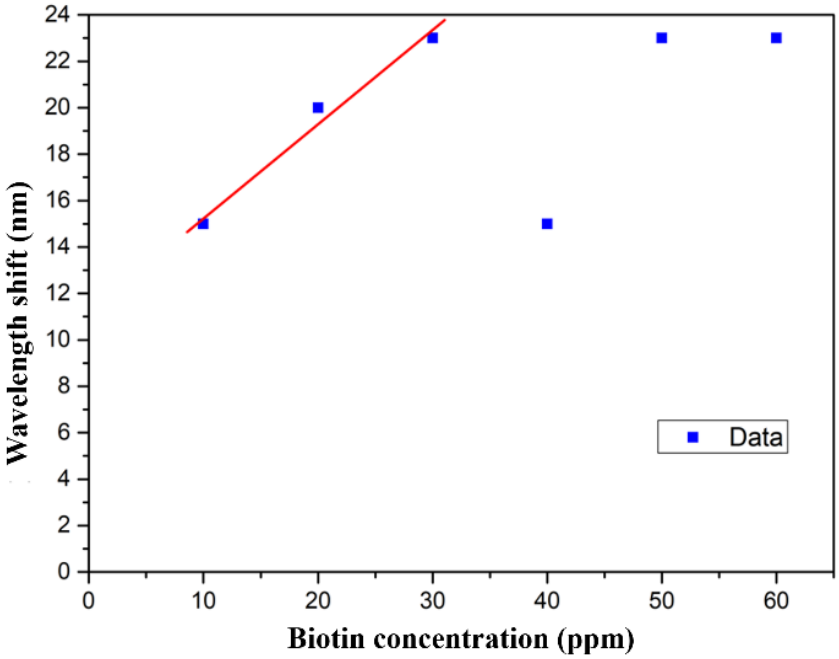

(a)

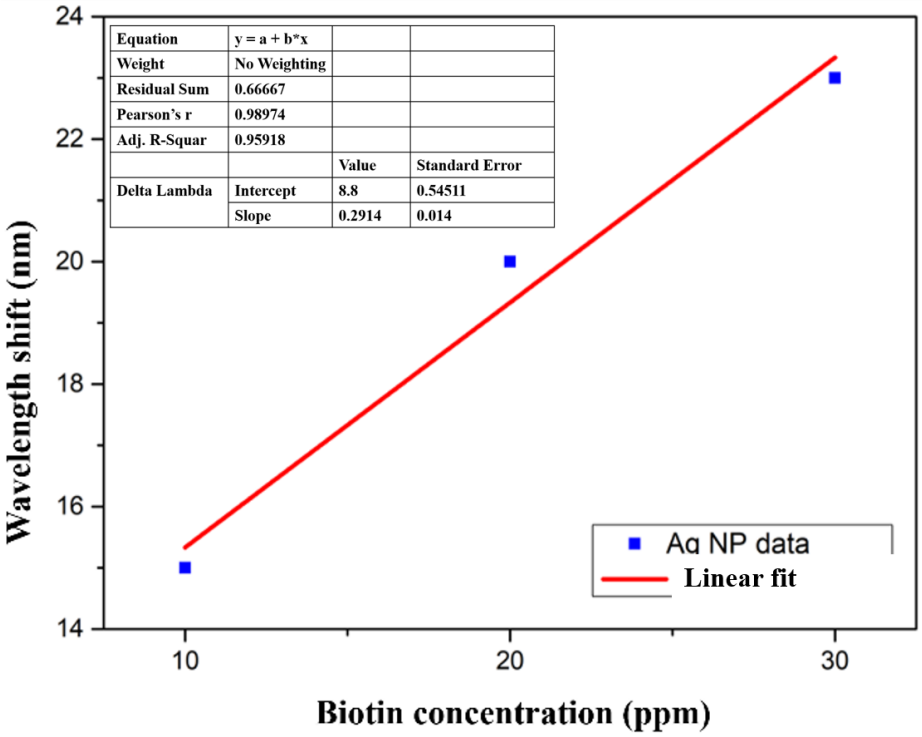

(b)

Fig. 6. (a) Variations in peak shifts arising from the attachment of Biotin molecules onto silver nanoparticles (Ag NPs) across diverse concentrations; (b) Differential peak shifts elicited by the attachment of Biotin at varying concentrations (10, 20, and 30 ppm) onto silver nanoparticles (Ag NPs) (color online)

Table 2 shows LSPR peak shifts due to the Biotin concentration change of Ag NPs. Fig. 6a and 6b show LSPR peak shifts after adding Biotin to Ag NPs. As can be seen from Fig. 6, the sensor properties of Ag NPs follow a linear trend for 10, 20, and 30 ppm biotin concentrations. However, at 40 ppm this trend was broken, and a constant wavelength shift was measured at 50 and 60 ppm.

3.2. Binding of Biotin to Au NPs

Au NPs were produced after 20 minutes (1200 laser pulses) of laser deposition. Different concentrations of Biotin molecules were attached to determine the sensor properties of Au NPs produced by the PLD mechanism. The first, 10, 20, 30, 40, 50, and 60 ppm Biotin solutions were prepared in distilled water. After preparing 60 ppm

Biotin solution as in Ag NPs, other concentrations were established by dilution. Before binding the biotin molecule to Au NPs, pure water was added to the produced film surface, and the absorption spectrum was taken by UV-Vis-NIR spectroscopy. Then, by adding different concentrations of Biotin molecules to Au NPs, the spectra were taken and the shift amounts were determined.

In Fig. 7, only Au NP, Au NP distilled water, Au NP, and Biotin molecules are added to NP film at different concentrations and LSPR peaks are seen. In Fig. 8, in the LSPR spectrum obtained by adding distilled water and 10, 20, 30, 40, 50, and 60 ppm biotin molecules with Au NP for 20 minutes (1200 laser pulses), it is seen that the peaks formed are shifted to the low wavelength (blue-shift) region.

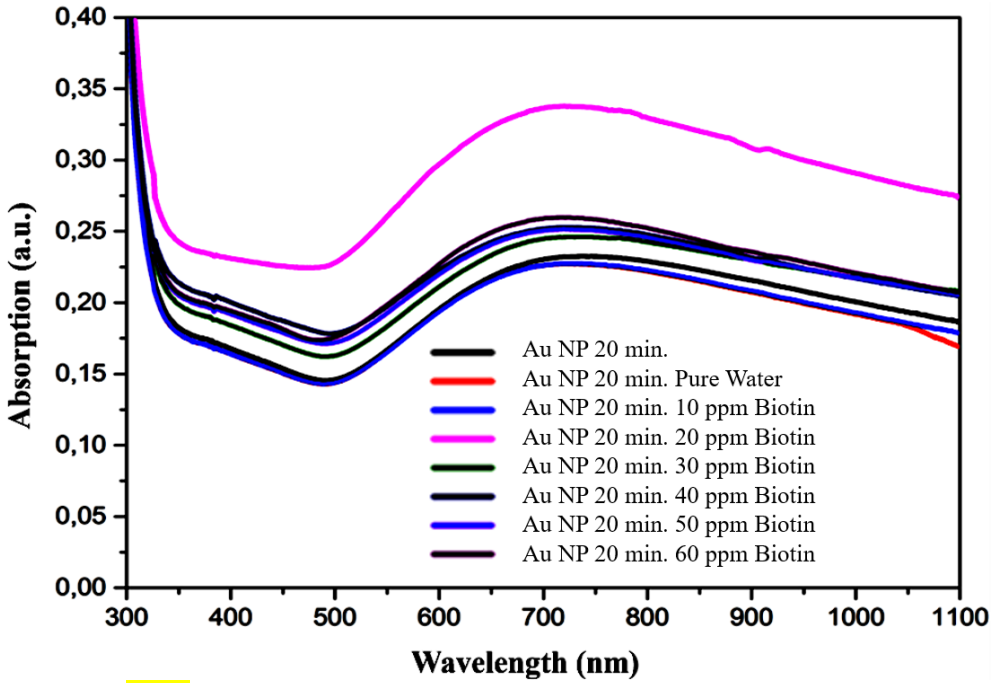

Fig. 7. LSPR peaks shifted blue after Biotin binding to Au NPs (color online)

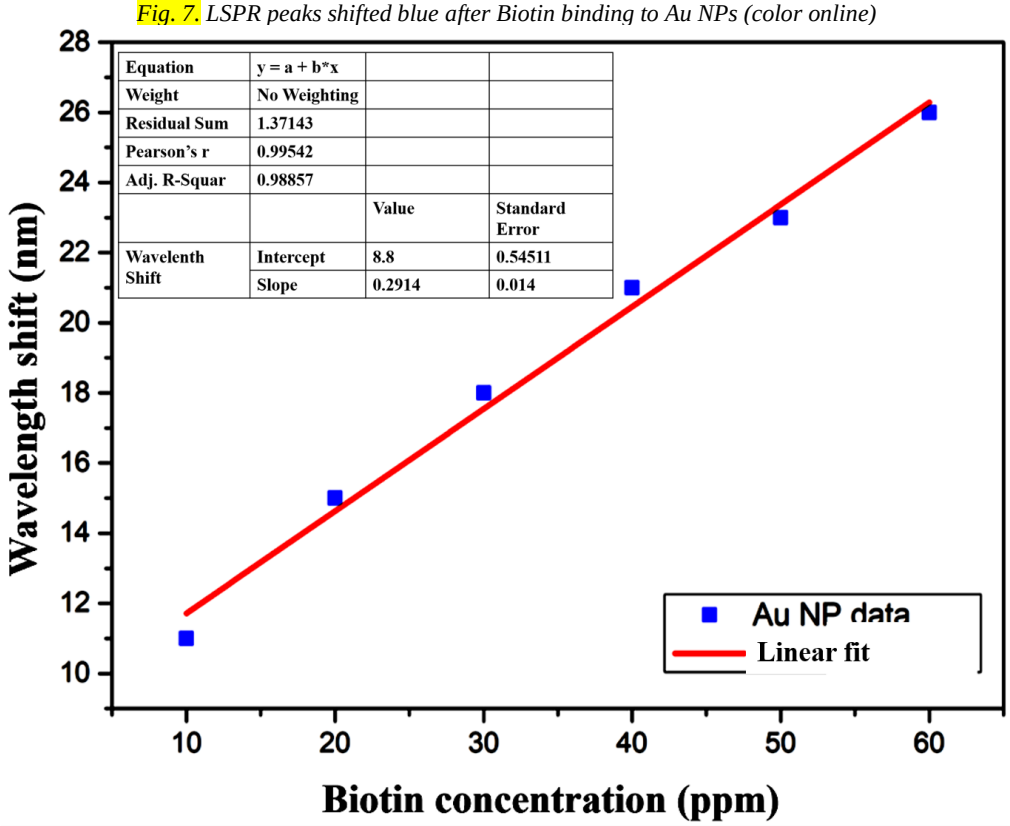

Fig. 8. LSPR peak shifts observed as a consequence of the interaction between various concentrations of Biotin molecules and gold nanoparticles (Au NPs) (color online)

Table 3. LSPR peak shifts of Au NPs due to Biotin concentration change

Element and Deposition time	**Binding molecule**	**Concentration (ppm)**	**Laser pulse number**	**NP Shape**	**LSPR Peak (nm)**	**$\Delta\lambda$(nm)**
Au NP 20 min	-	-	12000	Spherical	733	Reference peak
Au NP 20 min	Pure water	-	12000	Spherical	711	22
Au NP 20 min	Biotin	10	12000	Spherical	722	11
Au NP 20 min	Biotin	20	12000	Spherical	718	15
Au NP 20 min	Biotin	30	12000	Spherical	715	18
Au NP 20 min	Biotin	40	12000	Spherical	712	21
Au NP 20 min	Biotin	50	12000	Spherical	710	23
Au NP 20 min	Biotin	60	12000	Spherical	707	26

Fig. 8 shows LSPR peak shifts after adding Biotin to Au NPs. As can be seen from Fig. 8, the sensor properties of Au NPs follow a linear trend for 10, 20, 30, 40, 50, and 60 ppm biotin concentrations. The fact that the wavelength shift is directly proportional to the increase in concentration indicates that the linear detection ability of Au NPs is higher than that of Ag NPs. Therefore, Au NPs produced by the PLD mechanism are more capable of being used as sensors than Ag NPs. Table 3 shows LSPR peak shifts due to the Biotin concentration change of Ag NPs.

When the LSPR peaks of produced Au and Ag were examined by UV-Vis-NIR spectroscopy in air, it was observed that the peaks were red-shifted as the deposition time increased. Because, as the number of laser pulses increases, the produced NPs increase in size, causing LSPR peaks to be in the higher wavelength region of the spectrum (redshift). On the other hand, when pure water or molecules are added to the produced Ag and Au NPs, LSPR peaks that occur shift to the shorter wavelength, that is, the higher energy region (blue-shift). The reason for this is that when water and molecules are added, the refractive index of the environment in which NP is located increases, and thus the peak is shifted to blue. When the refractive index of the medium surrounding NP changes, the transmitted light is scattered more, shifting the LSPR peak to a lower wavelength.

In previous studies reported in the literature, it has been revealed that during the Au nanorods' growth, the peak position of LSPR shifted from 780 nm to 650 nm over the 60-minute period [45]. It experiences a constant blue shift as we observed in Fig. 7 and 8. In their study, it is argued that this behaviour is inconsistent with the nanorod growth mechanism's basic understanding. The position of the LSPR peak should display a red shift rather than a blue shift, assuming other parameters are kept unchanged, as the rods grow from spheres [49]. The reason is that nanorod length increases, and the electrons' confinement along the rod's long axis declines. As a consequence, the peak in the longitudinal axis should display a red shift [50]. Nevertheless, in our case, as we increase the concentration of the biotin, the LSPR peak position undertakes a continuous blue shift. Our findings can be compared with a previous study performed by Sau et al [51]. In their study, they have revealed that the LSPR position's behaviour is grounded merely on aspect ratio. On the other hand, Recio et al [52] took into account the surrounding medium's effect and revealed that the LSPR position's blue-shift could be described by considering the interaction between the electrons' collective longitudinal oscillation and the surrounding medium. Numerous investigations [53, 54] showed that surfactants could undertake reorganization based on thermodynamic environment and salt concentration, which can similarly affect the medium's dielectric constant. Furthermore, Link et al [49] correspondingly exposed the dielectric medium's immaculate contribution to the shift of LSPR peak by using theoretical calculations. Henceforth, it is obvious from these studies that it is not enough to explain the blue shift merely from a decrease in aspect ratio contrasting that presented by Sau et al [51], and the surrounding medium is needed to be taken into account as well [55].

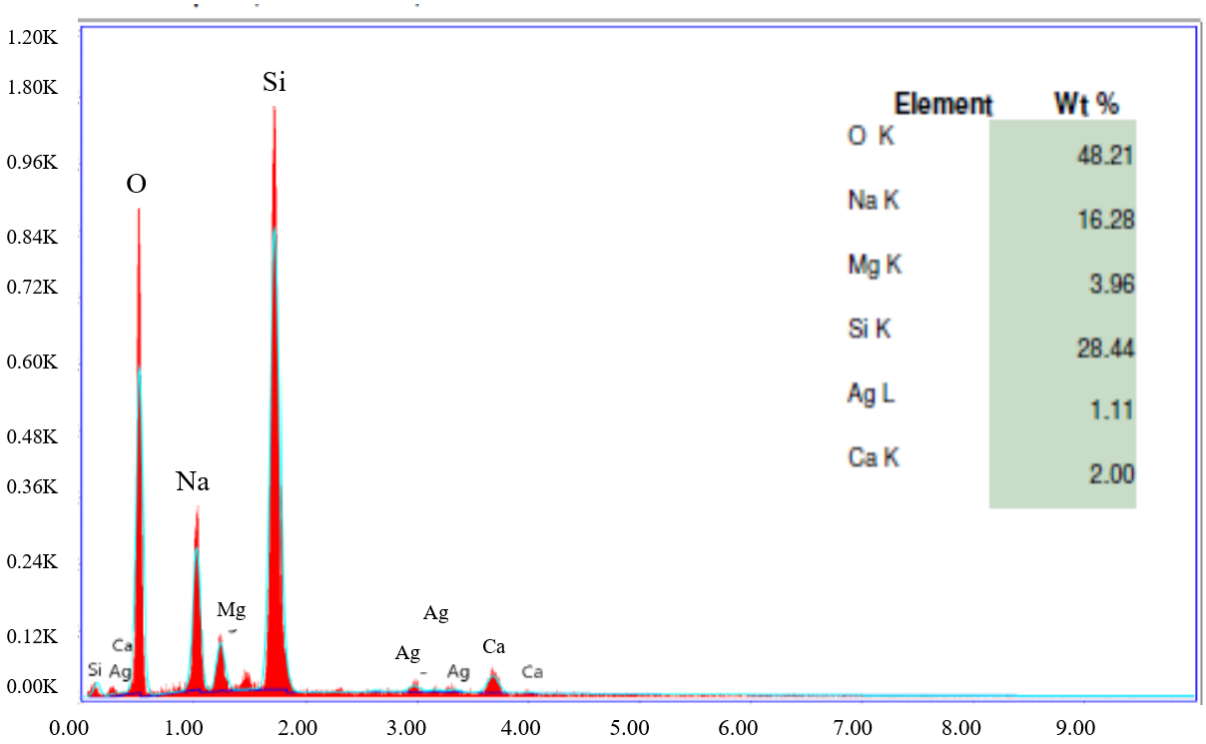

Fig. 9. EDX spectrum of Ag NPs thin film for 24 minutes (14400 laser pulses) (color online)

The content of elements in the EDX spectrum of Ag NP thin film for 24 minutes (14400 laser pulses) that are Ag, Si, O, Na, Ca, Na, and Mg as shown in Fig. 9. The Ag content proves that we used Ag target for the experiment, among other ingredients, when placing NPs on glass microscopic slides. The detailed wt% of the elements are given in the inside of Fig. 9. The EDX spectrum of Ag NPs produced for 14400 laser pulses is shown in Fig. 9. The content of thin film consists of Ag, Si, O, Na, Ca, Na and Mg. Ag NPs are deposited on glass microscope slides and EDX findings agree with the experimental setup.

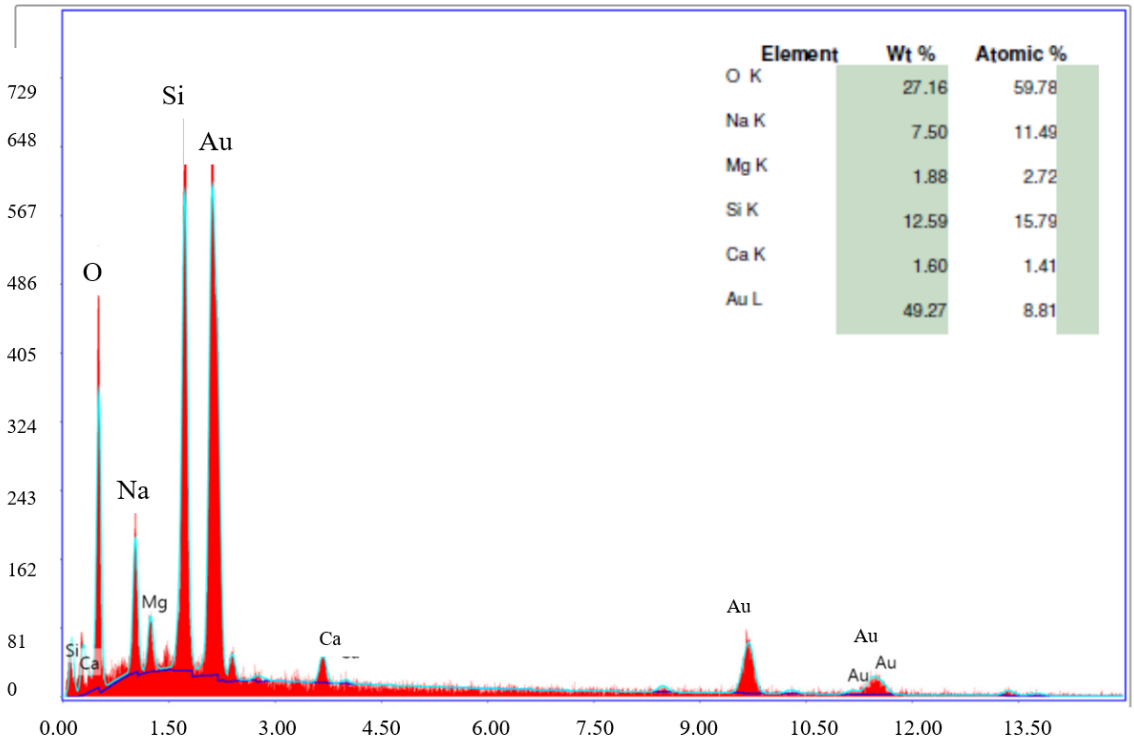

Fig. 10. EDX spectrum of Au NPs thin film produced for 12000 laser pulses (20 min) (color online)

The content of elements in EDX spectrum of Au NPs thin film produced for 12000 laser pulses (20 min) that are Au, Si, O, Na, Ca, Na and Mg. Au content proves that we used Au target for the experiment, among other ingredients, when placing NPs on the glass microscopic substrate. The wt% of the elements are given in the inside of Fig. 10. The EDX spectrum of Au NPs produced for 12000 laser pulses is shown in Fig. 10. The content of thin film consists of Au, Si, O, Na, Ca, Na and Mg. Au NPs are deposited on glass microscope substrates and EDX findings are in agreement with the experimental setup.

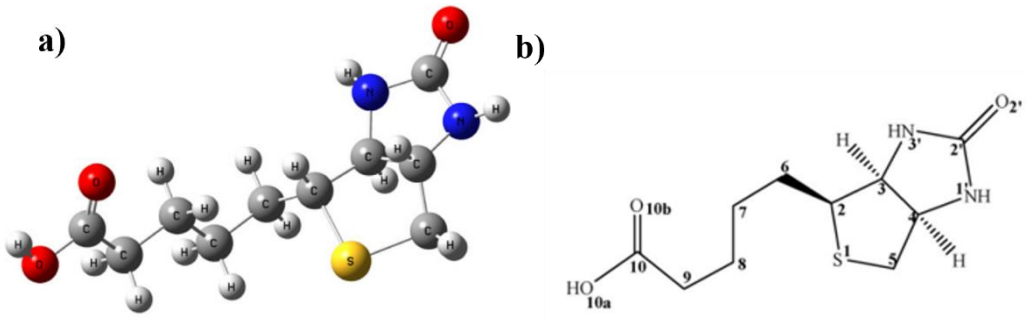

Fig. 11. (a) Optimized Biotin structure, (b) Chemical structure of Biotin [36] (color online)

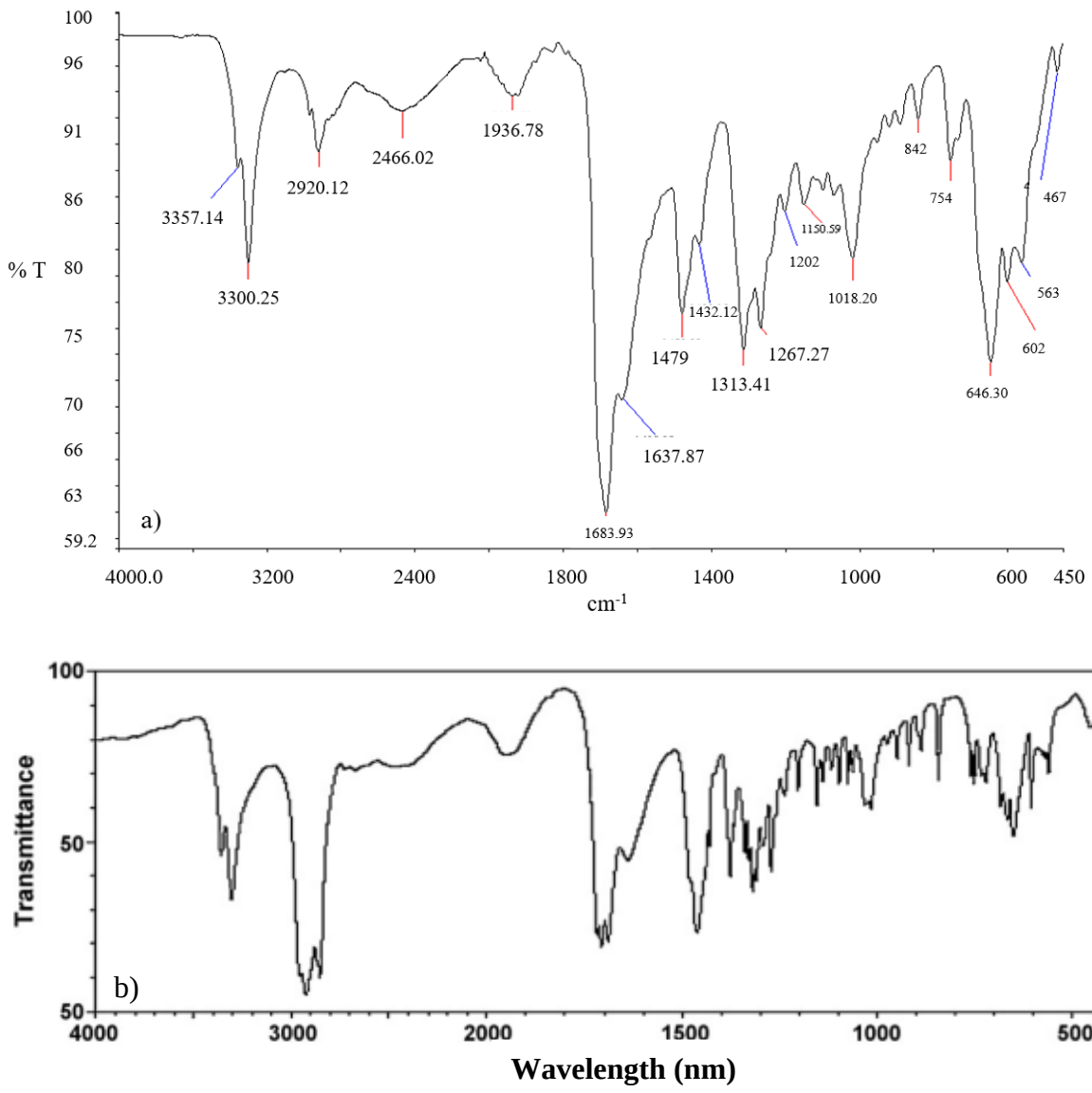

Fig. 12. a) Experimentally obtained FTIR spectrum of Biotin, b) Calculated FTIR spectrum of Biotin [36] (color online)

Fig. 12a shows the FTIR spectrum of biotin obtained experimentally in our study and Fig. 12b is a biotin's FTIR spectrum obtained in a previous study [36]. As can be seen in Fig. 12a and 12b, both spectra are in good agreement. O-H stretching vibration displays a band in the 3100-3400 cm^{-1} range. N-H stretching vibrations can additionally be seen within the same range. OH mode within 3325-3623 cm^{-1} can be observed based on ab-initio calculations. The stretching vibration of the C=O band appears at 1817 cm^{-1}. In-plane bending of OH occurs between 1390 and 1450 cm^{-1}, whereas out-of-plane bending happens between 850 and 975 cm^{-1} [56]. The medium band at 1430 cm^{-1} in the IR spectrum, and the range of 1407-1546 cm^{-1}, are similarly allocated to OH mode. The deformations of O-H out-of-plane in biotin spectra are detected in the 958-1048 cm^{-1} region. OH in-plane bending and out-of-plane bending vibrations combine with CC stretching, and CH out-of-plane bending modes, respectively. A single band characterizes carboxylic groups characteristically that appear in the 1700-1820 cm^{-1} range because of the CO stretching vibration. In the FT-IR spectrum, the bands at 1166 cm^{-1} are related to C-COOH stretching vibrations. There are two other vibrations of a characteristic carboxylic group that are in-plane C-O-H bending (ı(C-OH)), and C-O stretching (C-O) commonly observed at 1150-1450 cm^{-1} based on whether dimeric, monomeric, or other species with hydrogen-bond are existing. Frequently, the ı(C-OH) mode seems at a higher frequency than the (C-O) mode. The $-CH_2-$ group vibrations (wagging, scissoring, rocking, and twisting) contribute to numerous normal modes in the low-frequency domain. in the FT-IR spectrum, the bands detected at around 1430 cm^{-1} related to the $-CH_2-$ group scissoring deformation. The twisting, rocking, and wagging modes are scattered over a wide range[36].

4. Conclusion

Au and Ag NPs were deposited on a glass substrate using the PLD technique. LSPR peaks of the produced NPs were determined using UV-Vis-NIR spectroscopy. LSPR peaks of Au NPs shifted from the Vis region to the IR region as the laser deposition time increased. In addition, it was measured that LSPR peaks of the produced Ag NPs shifted from the blue wavelength side of the Vis region to the NIR region. Thus, it has been shown that the optical properties of Ag NPs can be tuned using the PLD technique.

The morphologies of the produced Au and Ag NPs were analysed using SEM. As a result of these analyses, it was shown that the shapes of both Au and Ag NPs are spherical. In addition, it has been proven that the size of the produced NPs and their density per unit surface increase as the number of laser pulses, that is, the deposition time, increases. Although the produced NPs varied in size within each film, it was observed that the average size of the NPs increased as the number of laser pulses increased. In addition, it was determined by SEM images that the produced Au and Ag NPs were embedded in the glass substrate with the effect of high kinetic energy and temperature in the plasma. Therefore, it has been shown that these NPs will have high durability when used as sensors.

To characterize the sensor properties of Ag and Au NPs we produced, pure water, Biotin molecules were added to the surfaces of NPs, and LSPR peak shifts were determined by UV-Vis-NIR spectroscopy. When LSPR peak shifts of Ag and Au NPs were compared in refractive index units, peak shifts of approximately 100 nm/RIU and 150 nm/RIU were found, respectively. Thus, it was determined that Au NPs provided more LSPR peak shifts than Ag NPs. As a result, Au NPs have been shown to be more sensitive as sensors. In addition, it was confirmed that Au NPs gave a better linear detection range than Ag NPs in the measurements made depending on the concentration.

In future studies; by binding different molecules to Ag and Au NPs, the sensor properties can be examined and also the sensitivity limits of the produced NPs can be determined. In addition, future studies can be made on increasing the efficiency by adding Ag and Au NPs to PV cells. LSPR peaks of NPs can be tuned and used both in sensor technology and to increase the efficiencies of PV materials in different spectral regions.

Acknowledgments

The authors would kindly like to thank to:

- Selcuk University, Scientific Research Projects (BAP) Coordination Office for the support with the number 15201070 and 19401140 projects,
- Selçuk University, High Technology Research and Application Center (İL-TEK) and
- SULTAN Center for infrastructures
- Dicle University Scientific Research Project (BAP) Coordination office

References

[1] C.-T. Liu, A.-N. Tang, Anal. Lett. **48**(7), 1031 (2015).
[2] N. Li, D. Liu, H. Cui, Anal. Bioanal. Chem. **406**(23), 5561 (2014).
[3] C. L. Haynes, and R. P. Van Duyne, The Journal of Physical Chemistry B, **105**(24), 5599-5611 (2001).
[4] A. R. Tao, S. Habas, P. Yang, small **4**(3), 310 (2008).
[5] E. Ringe, B. Sharma, A.-I. Henry, L. D. Marks, R. P. Van Duyne, Phys. Chem. Chem. Phys. **15**(12), 4110 (2013).
[6] A. Powell, M. Wincott, A. Watt, H. Assender, J. Smith, J. Appl. Phys. **113**(18), 184311 (2013).
[7] A. L. González, C. Noguez, A. S. Barnard, J. Mater. Chem. C **1**(18), 3150 (2013).
[8] T. Ahmad, I. A. Wani, J. Ahmed, O. A. Al-Hartomy, Appl. Nanosci. **4**(4), 491 (2014).
[9] W. A. Murray, B. Auguié, W. L. Barnes,

J. Phys. Chem. C. **113**(13), 5120 (2009).
[10] M. M. Miller, A. A. Lazarides, J. Phys. Chem. B. **109**(46), 21556 (2005).
[11] J. Chen, F. Saeki, B. J. Wiley, H. Cang, M. J. Cobb, Z. Y. Li, L. Au, H. Zhang, M. B. Kimmey, X. Li, Y. Xia,, Nano lett. **5**(3), 473 (2005).
[12] Y. Sun, B. Mayers, Y. Xia, Adv. Mater. **15**(7-8), 641 (2003).
[13] C. Loo, A. Lowery, N. Halas, J. West, R. Drezek, Nano lett. **5**(4), 709 (2005).
[14] C. W. Hsu, B. G. DeLacy, S. G. Johnson, J. D. Joannopoulos, M. Soljacic, Nano lett. **14**(5), 2783 (2014).
[15] J. Boken, S. Dalela, C. Sharma, D. Kumar, J. Chem. Eng. Process. Technol. **4**(8), 1 (2013).
[16] S. Thatai, P. Khurana, J. Boken, S. Prasad, D. Kumar, Microchem. J. **116**, 62 (2014).
[17] A. C. Templeton, W. P. Wuelfing, R. W. Murray, Acc. Chem. Res. **33(**1), 27 (2000).
[18] M. A. El-Sayed, Acc. Chem. Res. **34**(4), 257 (2001).
[19] L. N. Lewis, Chem. Rev. **93**(8), 2693 (1993).
[20] T. Tani, Silver nanoparticles: from silver halide photography to plasmonics, Oxford University Press, USA, (2015).
[21] S. R. Nicewarner-Pena, R. G. Freeman, B. D. Reiss, L. He, D. J. Peña, I. D. Walton, R. Cromer, C. D. Keating, M. J. Natan, Science **294**(5540), 137 (2001).
[22] S. A. Maier, M. L. Brongersma, P. G. Kik, S. Meltzer, A. A. Requicha, H. A. Atwater, Adv. Mater. **13**(19), 1501 (2001).
[23] P. V. Kamat, J. Phys. Chem. B., **106**(32), 7729 (2002).
[24] C. Murray, S. Sun, H. Doyle, T. Betley, MRS Bulletin **26**(12), 985 (2001).
[25] S. Nie, S. R. Emory, Science **275**(5303), 1102 (1997).
[26] L. A. Dick, A. D. McFarland, C. L. Haynes, R. P. Van Duyne, J. Phys. Chem. B. **106**(4), 853 (2002).
[27] I. Candan, Sensor fabrication and analysis based on plasmonic noble metal (Au, Ag) nanoparticles, Dicle University, PhD Thesis (2022).
[28] S. Y. Gezgin, A. Kepceoğlu, H. Ş. Kılıç, AIP Conf. Proceedings **1815**(1), 030019 (2017).
[29] S. Y. Gezgin, A. Kepceoğlu, H. Ş. Kılıç, AIP Conf. Proceedings **1815**(1), 030020 (2017).
[30] S. Yiğit Gezgin, H. Ş. Kiliç, Indian Journal of Physics **97**(3),779 (2023).
[31] J. Zempleni, D. Mock, J. Nutr. Biochem. **10**(3), 128 (1999).
[32] E. Regula Baumgartner, T. Suormala, Biofactors, **10**(2-3), 287 (1999).
[33] D. Koutsikos, B. Agroyannis, H. Tzanatos-Exarchou, Biomed. Pharmacother. **44**(10), 511 (1990).
[34] J. R. Knowles, Annu. Rev. Biochem. **58**(1), 195 (1989).
[35] P. M. Debourdeau, S. Djezzar, J. L. F. Estival, C. M. Zammit, R. C. Richard, A. C. Castot, Ann. Pharmacother. **35**(4), 424 (2001).
[36] M. Emami, A. Teimouri, A. N. Chermahini, Spectrochim. Acta A Mol. Biomol. Spectrosc. **71**(4), 1516 (2008).
[37] İ. Candan, S. Y. Gezgin, Y. Gündoğdu, H. B. Gümgüm, Middle East J. Sci. **7**(2), 112 (2021).
[38] E. Martinsson, Nanoplasmonic sensing using metal nanoparticles, Linköping University Electronic Press, 2014.
[39] X. Huang, M. A. El-Sayed, J. Adv. Res. **1**(1), 13 (2010).
[40] M. A. García, J. Phys. D **44**(28), 283001 (2011).
[41] C. Noguez, J. Phys. Chem. C. **111**(10), 3806 (2007).
[42] S. Y. Gezgin, H. Ş. Kılıç, A. Kepceoğlu, S. Bayır, İ. E. Nalbantoğlu, A. Toprak, AIP Conf. Proceedings **1722**(1), 200013 (2016).
[43] S. Y. Gezgin, A. Houimi, H. Ş. Kılıç, Optik **199**(163370), 163370 (2019).
[44] S. Y. Gezgin, A. Houimi, Y. Gündoğdu, B. Mercimek, H. Ş. Kılıç, Vacuum **192**, 110451 (2021).
[45] A. Shafiqa, A. A. Aziz, B. Mehrdel, J. Phys. Conf. Ser.: IOP Publishing **108**(1), 012040 (2018).
[46] E. Boulais, R. Lachaine, A. Hatef, M. Meunier, J. Photochem. Photobiol. C **17**, 26 (2013).
[47] S. Y. Gezgin, A. Kepceoğlu, Y. Gündoğdu, S. Zongo, A. Zawadzka, H. Sükür Kilic, B. Sahraoui, Nanomaterials **10**(6), 1071 (2020)
[48] W. Haiss, N. T. Thanh, J. Aveyard, D. G. Fernig, Anal. Chem. **79**(11), 4215 (2007).
[49] S. Link, M. B. Mohamed, M. El-Sayed, J. Phys. Chem. B. **103**(16), 3073 (1999).
[50] E. B. Guidez, C. M. Aikens, Nanoscale **6**(20), 11512 (2014).
[51] T. K. Sau, C. J. Murphy, Langmuir **20**(15), 6414 (2004).
[52] F. J. Recio, N. Zabala, A. Rivacoba, P. Crespo, A. Ayuela, P. M. Echenique, A. Hernando, J. Phys. Chem. C **119**(14), 7856 (2015)
[53] W. Li, M. Zhang, J. Zhang, Y. Han, Front. Chem. **1**, 438 (2006).
[54] P. Sarkar, A. Chattopadhyay, Chem. Phys. Lipids **195**, 34 (2016).
[55] A. K. Sahu, A. Das, A. Ghosh, S. Raj, Nano Express **2**(1), 010009 (2021).
[56] M. Alcolea Palafox, Int. J. Quantum Chem. **77**(3), 661 (2000).

*Corresponding author: hamdisukurkilic@selcuk.edu.tr